

# archi|DOCT

*The e-journal for the  
dissemination of doctoral  
research in architecture*

**July 2019**

[www.archidoct.net](http://www.archidoct.net)

**ISSN 2309-0103**

**13**  
**FORCES**

Listed in:  
**Scopus®**

## **(De)constructing and analysing a joint**

Hector Cantos Coronel // ETS Arquitectura del Vallès, Universitat Politècnica de Catalunya

### **Abstract**

*This paper discusses the possibility of designing a pin joint that is also easy to fasten in position in order to support the stresses of a conventional and not lightweight structure. It is believed that it is possible to prefabricate a structural system based on a Hexagrid configuration that can be folded, transported, deployed and assembled. The model is produced by means of a process that goes from geometric functional design of the joint to validation of its structural resistance using a finite element model through which stresses and deformations will be analysed in order to find a stable solution that is feasible to build.*

### **Keywords**

Hexagrid; Joint; Foldable; Modular



## 1. Introduction

The content of this article is part of broader research that attempts to find a prefabricated and transportable structural system to be implemented in areas of Latin America, where technology is concentrated around large cities but where there is a great need to create new infrastructure in areas relatively far from development poles, where there are no facilities to implement modern building systems.

### 1.1 *Using tubular systems*

The systematic development of tubular structural systems in buildings started in the Master's thesis completed by Myron Goldsmith in 1953, under the supervision of Mies Van de Rohe, at the Illinois Institute of Technology, Chicago. That thesis proposed three types of tube structure: variable irregular Diagrid frame, narrow regular Diagrid frame and a solution of mega-trusses (Goldsmith, 1953). Fazlur Rhaman Khan paid greater attention to the development of the mega-truss system, while the other two systems proposed have been developed more recently, since construction technology has allowed it and since the need to achieve taller buildings with more complex volumes has demanded it (Montuori, 2015).

### 1.2 *The Diagrid system*

The Diagrid system consists of a tubular structure composed solely of diagonal bars that are capable of transporting the vertical and lateral forces of a building without columns. Its diamond configuration, together with the rigidity of the slabs, allows axial behaviour of the forces in the bars, which makes it a very efficient system that at the same time has great aesthetic potential in the design of architectural elements. Since the beginning of the 21st century, architect Norman Foster and ARUP have used the Diagrid concept in their designs<sup>1</sup> (Boake, 2013) and it has started to become used more frequently to resolve high-rise building structures.

### 1.3 *The Hexagrid system*

Operating in antithesis to the mainstream<sup>2</sup> (HTA Association, 2007), the development of an architectural language based on hexagons has gathered momentum over time in a non-linear yet continuous way, taking as examples Buckminster Fuller's geodesic frames seen at the 1957 World's Fair in Montreal or the contemporary Islamic architecture of Zvi Hecker with Alfred Neumann. One of the major reasons for using hexagonal frames in architecture is based on verifying the honeycomb conjecture, which was mathematically demonstrated at the end of the twentieth century. The conjecture states that a regular hexagonal grid is the best way to divide a surface into regions of equal area with the least total perimeter (Hales, 1999).

The HTA Association hypothesised that a tube structural system might be developed based on hexagonal modular frames that are rigid enough to be considered viable for use in the construction of building structures. This system was called honeycomb tube. The honeycomb tube system demonstrated as a way of designing and building at all scales is explained, from planning to possible application, in three informative books<sup>3 4 5</sup>.

#### 1.4 *Foldability of structural frames*

The idea of packaging complete sections of structure to reduce their volume is nothing new. In fact, for lightweight structures there are several solutions based on bars that can be folded for transport and then deployed and placed in situ (Escrig, 2013).

Although there are certain types of structural framework with the capacity to stabilise their position of use, normally at the cost of subjecting their elements to great stresses during the deployment process (Franco, 2010), which can even lead to deformation of the structure, such as the experimental developments of Bricard linkages (Chen, 2003), the majority of frames need elements to be added in order to stabilise their shape and behaviour as a structure, either in the form of cables or bars. A framework may be stabilised by changing a pin joint to a fixed joint. This task often requires complex designs that adapt to the scale, building possibilities and stresses that the structure will have to support. In the search for pin joints that can be stable in their position of use, we have looked at joint patents at different scales, ranging from camera tripods<sup>6</sup> to the design of lightweight structures<sup>7 8 9</sup>.

### 2. Description of the structure to be resolved

Within a set of previously developed and analysed multi-storey building models, ranging from four floors to 15 floors, the tallest possible building height for the proposed conditions is taken as a sample. This square-based building has a volume contained in a parallelepiped, the dimensions of which are 16.17 m by 16.17 m at the base by 52.5 m height. The structural layout is tubes within tubes, which spreads the load distribution between the perimeter structure and a core. The perimeter tubular system is made up of four surfaces identical in their geometry and the load distribution means that each face is subject to equivalent stresses, with behaviour and deformation that can be correlated. Each surface is composed of a horizontal hexagonal frame five hexagonal modules wide by 15 hexagonal modules high. Of all the joints and bars that make up the perimeter frames, joint number 14, corresponding to the intersection of bars 11, 12 and 17, was chosen as a reference. The choice of this joint is justified in the structural analysis indicating that, within the type of joints receiving three bars, it is this joint in which the greatest amount of stress is concentrated (Figure 1 and Figure 2).

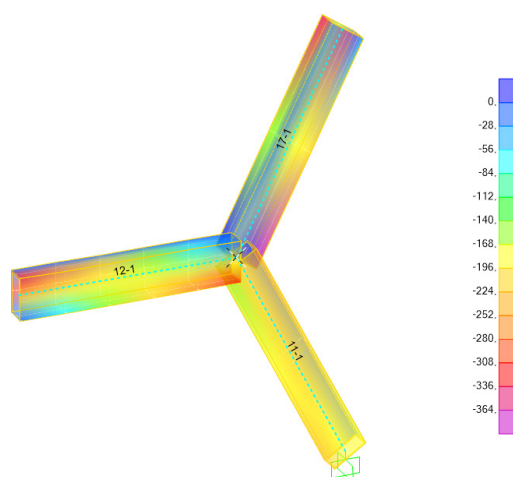
#### 2.1 *Choice of profile type*

The profiles used are rectangular hollow tubes, similar to those used in analyses conducted by other authors (Montuori, et al., 2015) and (de Meijer, 2012), as they simplify the joint design and also work for structures subject to bending and compression.

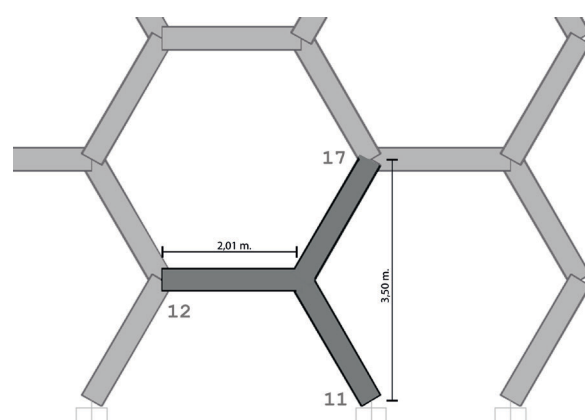
### 3. Frame folding method

With a Hexagrid we are looking for a packaging system that, by taking advantage of the vacuum that exists between bars, reduces the volume of the frame as much as possible, with the intention of being able to transport sections of frame as large as possible, reducing and simplifying the assembly work required on the building site (Figure 3 and Figure 4).

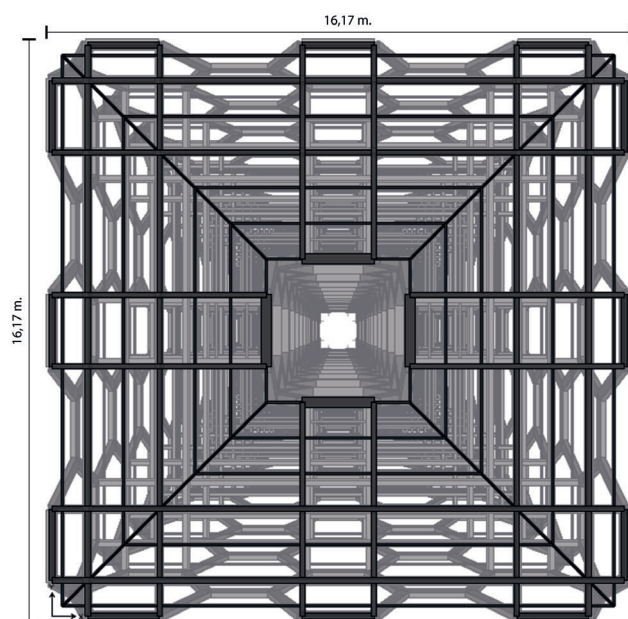


**Figure 1.**

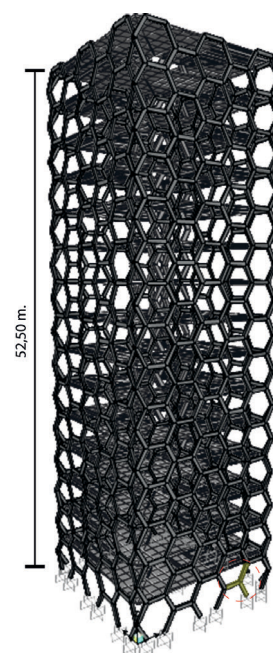
Bars 11, 12 and 17 stress diagram (N/mm<sup>2</sup> SII Max/Min.  
UDSTL7)

**Figure 2.**

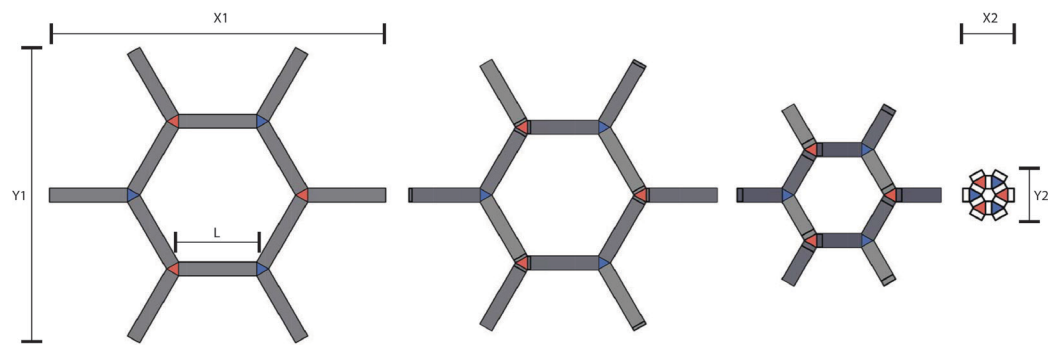
Joint no. 14. Intersection of bars 11, 12 and 17

**Figure 3.**

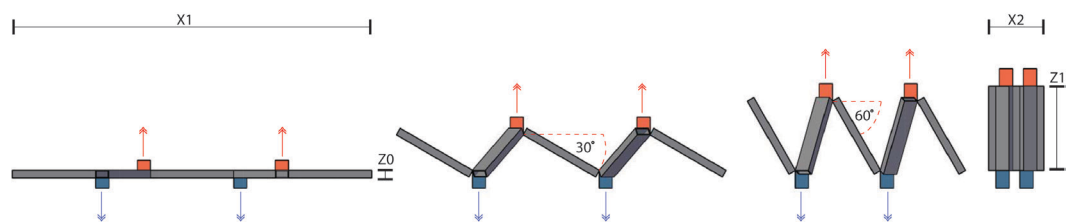
Hexagrid building structure, floor plan distribution

**Figure 4.**

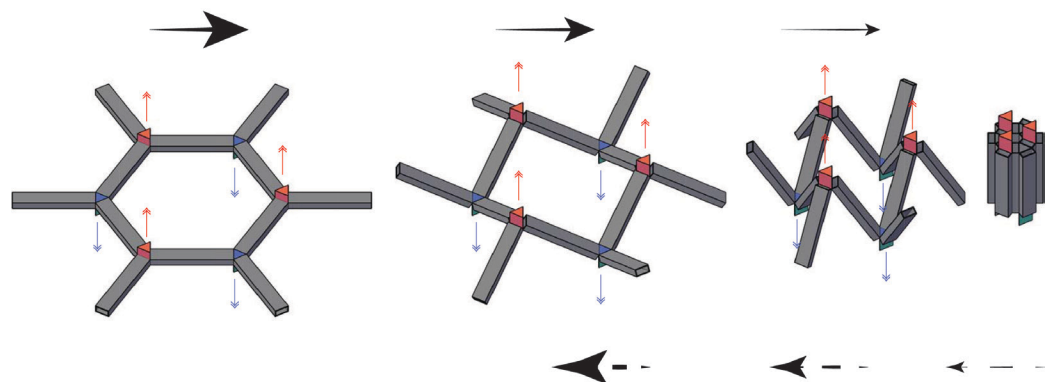
Hexagrid building structure, axonometric

**Figure 5.**

Conceptual folding of the system, plan view

**Figure 6.**

Conceptual folding of the system, elevation view

**Figure 7.**

Conceptual folding of the system, axonometric

### 3.1 *The folding system*

The frame is defined as an ordered set of joints connected by means of bars that form a surface that extends in the X plane, and with measurements  $X1, Y1$  and  $Z0$  modulated by means of regular hexagons, each side of which has the same L dimension. The intention of the folding system is that by rotating each articulation connecting the three arms that make up the joint with their respective bars, the frame is transformed into a volume with measurements  $X2, Y2$  and  $Z1$  so that measurements  $X2$  and  $Y2$  are smaller than  $X1$  and  $Y1$ , tending hypothetically to zero, while  $Z1$  reaches a measurement similar to L. To validate the folding method, it must be possible to return to the frame's initial state (Figure 5, Figure 6 and Figure 7).

## 4. Joint design conditions and limitations

In order to meet the expectations of the mechanism/structure duality, the design of a hybrid joint with the following characteristics is required:

- Simple mechanisms with simple fastening methods.
- Small number of parts.
- Standardisation of parts.
- Possibility of replicating and adapting the model to different load requirements within the logic of the system.

The design process takes into account that the material used will be S355 steel joined by welding and that connections with bars will be done using bolts.

### 4.1 *Scope of the design*

Three types of joints are required to assemble the Hexagrid frame:

A: a joint that receives three equal bars, one along each arm, forming an angle of 120 degrees between any bar and its adjacent bar.

B: a joint connecting the structure to the foundations.

C: a joint at the edge of the structural frame that receives two bars and connects the frame with its adjacent frame at the corners.

This article will look at joint type A, since types B and C may be considered designs derived from the original model.

## 5. Designing the joint type A

The design methodology applied corresponds to linear and delimited phases. A more in-depth description of the design phases is explained below.

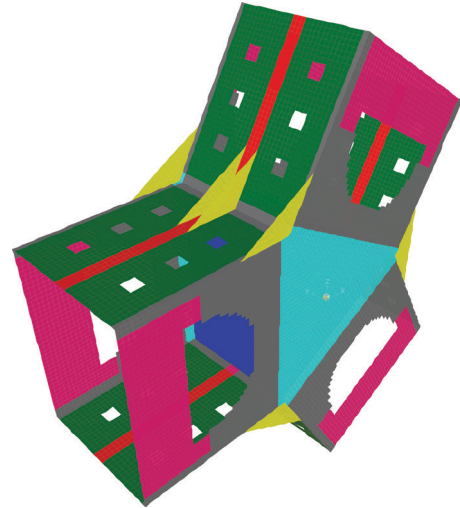
### 5.1 *Geometric and functional design*

From the dimensions taken from the building model, a series of joint models are made that evolve to a level that meets the proposed conditions. Each piece of the model takes a section thickness within the range of 80% to 120% of the section thickness of the bars. In order to look at the joint and check the way it operates, a 1:5 scale model is printed in 3D, in which the pros and cons of the model are noted for correction.



**Figure 8.**

Model of finite modules by colour for the application of section thicknesses

**Figure 9.**

Model of finite modules with section thicknesses applied

| Finite element thickness applications |          |                 |        |        |       |
|---------------------------------------|----------|-----------------|--------|--------|-------|
| Group                                 | Layer    | Thickness (mm.) |        |        |       |
|                                       |          | Bar             | Part A | Part B | Total |
| 1                                     | Red      | 12.5            | 12.5   |        | 25.0  |
| 2                                     | Yellow   |                 |        | 8.0    | 8.0   |
| 3                                     | Green    | 12.5            | 12.5   | 10.0   | 35.0  |
| 4                                     | Sky blue |                 |        | 10.0   | 10.0  |
| 5                                     | Blue     |                 |        |        | 0.0   |
| 6                                     | Lilac    | 12.5            |        |        | 12.5  |
| 7                                     | Grey     | 12.5            |        | 10.0   | 22.5  |

**Table 1.**

Distribution of section thicknesses in finite element models

| Bar | Flange | Colour   |
|-----|--------|----------|
| 11  | A      | Lilac    |
|     | B      | Yellow   |
| 12  | A      | Grey     |
|     | B      | Blue     |
| 17  | A      | Green    |
|     | B      | Sky blue |

**Table 2.**

Colours of force application groups per bar

**Figure 10.**

Location of force application points in joint type

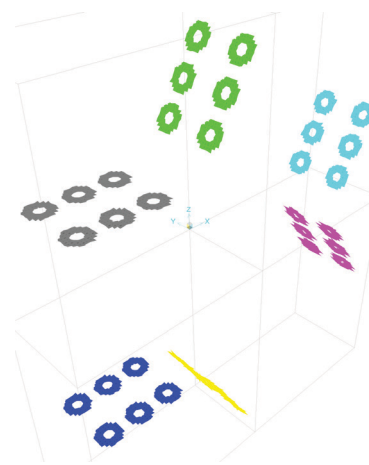
**Figure 11.**

Diagram of force application groups explained in colour

### 5.2 Constructing the finite element model

The aim is to be able to transform the results of the search process into a comparable yet simplified model that can be made in design<sup>10</sup> software and entered into the interface of the structural analysis software<sup>11</sup>. We have created a three-dimensional model composed of two-dimensional finite elements, assigning the material corresponding to S355 steel to these modules, with the determined thickness. In order to facilitate the application of section thickness properties, different layers corresponding to a specific thickness are used (Figure 8, Figure 9 and Table 1).

### 5.3 Force application area

The equivalent forces of each bar are distributed in the upper and lower flanges of each of the model's arms, causing the joint loads to be distributed across the vertexes of the finite elements around the holes through which the joint parts would be connected to the bars via pins (Table 2). The forces are distributed between 384 points per group on each flange on each of the arms (Figure 10 Figure 11).

### 5.4 Obtaining forces

From the previous analysis of the overall building model, numerical stress data is obtained for nine load cases corresponding to bars 11, 12 and 17 in the joint from the building model (Table 3).

| Frame | Joint | Output Case | F1       | F2     | F3       | M1     | M2      | M3    |
|-------|-------|-------------|----------|--------|----------|--------|---------|-------|
| Text  | Text  | Text        | KN       | KN     | KN       | KN-m   | KN-m    | KN-m  |
| 11    | 14    | UDSTL10     | 1236.89  | -18.04 | -2405.28 | -1.88  | 133.40  | -8.15 |
| 12    | 14    | UDSTL10     | -2510.33 | 0.34   | -13.39   | -0.28  | -16.19  | -0.22 |
| 17    | 14    | UDSTL10     | 1273.44  | 17.70  | 2418.67  | 2.16   | -117.21 | 8.37  |
| 11    | 14    | UDSTL2      | 955.14   | -10.71 | -1824.85 | -6.90  | 86.43   | -5.03 |
| 12    | 14    | UDSTL2      | -1910.71 | 0.14   | 0.80     | -0.11  | -0.34   | 0.22  |
| 17    | 14    | UDSTL2      | 955.58   | 10.57  | 1824.05  | 7.01   | -86.09  | 4.81  |
| 11    | 14    | UDSTL3      | 1125.05  | -9.86  | -2062.61 | -6.31  | 66.34   | -4.42 |
| 12    | 14    | UDSTL3      | -2086.89 | 0.43   | 95.97    | -0.35  | 95.49   | -0.07 |
| 17    | 14    | UDSTL3      | 961.84   | 9.43   | 1966.65  | 6.67   | -161.83 | 4.49  |
| 11    | 14    | UDSTL4      | 785.23   | -11.56 | -1587.08 | -7.49  | 106.52  | -5.65 |
| 12    | 14    | UDSTL4      | -1734.54 | -0.15  | -94.37   | 0.13   | -96.18  | 0.52  |
| 17    | 14    | UDSTL4      | 949.31   | 11.71  | 1681.45  | 7.36   | -10.34  | 5.13  |
| 11    | 14    | UDSTL5      | 753.32   | -5.78  | -1414.25 | -9.58  | 55.44   | -2.92 |
| 12    | 14    | UDSTL5      | -1485.50 | 0.00   | 9.24     | 0.00   | 9.10    | 0.49  |
| 17    | 14    | UDSTL5      | 732.18   | 5.78   | 1405.01  | 9.58   | -64.54  | 2.43  |
| 11    | 14    | UDSTL6      | 1156.95  | -15.64 | -2235.44 | -4.22  | 117.43  | -7.15 |
| 12    | 14    | UDSTL6      | -2335.93 | 0.27   | -7.64    | -0.22  | -9.79   | -0.04 |
| 17    | 14    | UDSTL6      | 1178.97  | 15.37  | 2243.08  | 4.45   | -107.64 | 7.19  |
| 11    | 14    | UDSTL7      | 1183.72  | -8.41  | -2117.24 | -5.36  | 48.26   | -3.60 |
| 12    | 14    | UDSTL7      | -2095.27 | 0.60   | 159.30   | -0.50  | 159.27  | -0.28 |
| 17    | 14    | UDSTL7      | 911.55   | 7.81   | 1957.94  | 5.85   | -207.53 | 3.88  |
| 11    | 14    | UDSTL8      | 617.36   | -11.25 | -1324.68 | -7.31  | 115.23  | -5.65 |
| 12    | 14    | UDSTL8      | -1508.01 | -0.37  | -157.93  | 0.30   | -160.17 | 0.71  |
| 17    | 14    | UDSTL8      | 890.66   | 11.62  | 1482.61  | 7.01   | 44.95   | 4.94  |
| 11    | 14    | UDSTL9      | 564.18   | -1.62  | -1036.64 | -10.80 | 30.09   | -1.10 |
| 12    | 14    | UDSTL9      | -1092.95 | -0.11  | 14.75    | 0.09   | 15.28   | 0.65  |
| 17    | 14    | UDSTL9      | 528.77   | 1.73   | 1021.89  | 10.71  | -45.37  | 0.45  |

**Table 3.**

Resisted forces in joint type, extracted from the building model



**Table 4.**  
Forces applicable (FApl) to joint type  
model

| Frame<br>Text | Joint<br>Text | Output Case<br>Text | F(A)Apl. kN |        |         | F(B)Apl. kN |        |         |
|---------------|---------------|---------------------|-------------|--------|---------|-------------|--------|---------|
|               |               |                     | F1A         | F2A    | F3A     | F1B         | F2B    | F3B     |
| 11            | 14            | UDSTL10             | 759.61      | -20.97 | -958.13 | 759.61      | -31.57 | -958.13 |
| 12            | 14            | UDSTL10             | -1255.16    | 0.50   | 27.57   | -1255.16    | -1.10  | 27.57   |
| 17            | 14            | UDSTL10             | 760.75      | 20.47  | 994.50  | 760.75      | 32.67  | 994.50  |
| 11            | 14            | UDSTL2              | 569.03      | 3.49   | -754.01 | 569.03      | -35.50 | -754.01 |
| 12            | 14            | UDSTL2              | -955.36     | 0.86   | 1.13    | -955.36     | 0.23   | 1.13    |
| 17            | 14            | UDSTL2              | 568.89      | -4.34  | 754.24  | 568.89      | 35.28  | 754.24  |
| 11            | 14            | UDSTL3              | 632.73      | 3.55   | -909.71 | 632.73      | -32.12 | -909.71 |
| 12            | 14            | UDSTL3              | -1043.44    | 1.05   | -154.11 | -1043.44    | -0.94  | -154.11 |
| 17            | 14            | UDSTL3              | 652.17      | -4.61  | 686.71  | 652.17      | 33.05  | 686.71  |
| 11            | 14            | UDSTL4              | 505.33      | 3.42   | -598.30 | 505.33      | -38.89 | -598.30 |
| 12            | 14            | UDSTL4              | -867.27     | 0.67   | 156.36  | -867.27     | 1.39   | 156.36  |
| 17            | 14            | UDSTL4              | 485.60      | -4.08  | 821.76  | 485.60      | 37.50  | 821.76  |
| 11            | 14            | UDSTL5              | 435.32      | 17.99  | -605.52 | 435.32      | -36.12 | -605.52 |
| 12            | 14            | UDSTL5              | -742.75     | 1.03   | -14.64  | -742.75     | 1.03   | -14.64  |
| 17            | 14            | UDSTL5              | 434.38      | -19.01 | 584.22  | 434.38      | 35.10  | 584.22  |
| 11            | 14            | UDSTL6              | 702.74      | -11.01 | -902.49 | 702.74      | -34.88 | -902.49 |
| 12            | 14            | UDSTL6              | -1167.96    | 0.69   | 16.89   | -1167.96    | -0.58  | 16.89   |
| 17            | 14            | UDSTL6              | 703.39      | 10.32  | 924.25  | 703.39      | 35.46  | 924.25  |
| 11            | 14            | UDSTL7              | 642.93      | 3.31   | -970.16 | 642.93      | -26.96 | -970.16 |
| 12            | 14            | UDSTL7              | -1047.63    | 1.10   | -257.43 | -1047.63    | -1.70  | -257.43 |
| 17            | 14            | UDSTL7              | 675.38      | -4.41  | 598.60  | 675.38      | 28.66  | 598.60  |
| 11            | 14            | UDSTL8              | 430.61      | 3.08   | -451.14 | 430.61      | -38.25 | -451.14 |
| 12            | 14            | UDSTL8              | -754.01     | 0.46   | 260.03  | -754.01     | 2.17   | 260.03  |
| 17            | 14            | UDSTL8              | 397.77      | -3.54  | 823.69  | 397.77      | 36.08  | 823.69  |
| 11            | 14            | UDSTL9              | 313.93      | 27.36  | -463.17 | 313.93      | -33.64 | -463.17 |
| 12            | 14            | UDSTL9              | -546.48     | 1.06   | -24.97  | -546.48     | 1.57   | -24.97  |
| 17            | 14            | UDSTL9              | 312.40      | -28.42 | 427.78  | 312.40      | 32.07  | 427.78  |

**Table 5.**  
Point forces applicable (FApl.point) to  
joint type model

| Frame<br>Text | Joint<br>Text | Output Case<br>Text | F(A)Apl.point<br>(384 points) kN |        |        | F(B)Apl.point<br>(384 points) kN |        |        |
|---------------|---------------|---------------------|----------------------------------|--------|--------|----------------------------------|--------|--------|
|               |               |                     | F1A                              | F2A    | F3A    | F1B                              | F2B    | F3B    |
| 11            | 14            | UDSTL10             | 1.978                            | -0.055 | -2.495 | 1.978                            | -0.082 | -2.495 |
| 12            | 14            | UDSTL10             | -3.269                           | 0.001  | 0.072  | -3.269                           | -0.003 | 0.072  |
| 17            | 14            | UDSTL10             | 1.981                            | 0.053  | 2.59   | 1.981                            | 0.085  | 2.59   |
| 11            | 14            | UDSTL2              | 1.482                            | 0.009  | -1.964 | 1.482                            | -0.092 | -1.964 |
| 12            | 14            | UDSTL2              | -2.488                           | 0.002  | 0.003  | -2.488                           | 0.001  | 0.003  |
| 17            | 14            | UDSTL2              | 1.481                            | -0.011 | 1.964  | 1.481                            | 0.092  | 1.964  |
| 11            | 14            | UDSTL3              | 1.648                            | 0.009  | -2.369 | 1.648                            | -0.084 | -2.369 |
| 12            | 14            | UDSTL3              | -2.717                           | 0.003  | -0.401 | -2.717                           | -0.002 | -0.401 |
| 17            | 14            | UDSTL3              | 1.698                            | -0.012 | 1.788  | 1.698                            | 0.086  | 1.788  |
| 11            | 14            | UDSTL4              | 1.316                            | 0.009  | -1.558 | 1.316                            | -0.101 | -1.558 |
| 12            | 14            | UDSTL4              | -2.259                           | 0.002  | 0.407  | -2.259                           | 0.004  | 0.407  |
| 17            | 14            | UDSTL4              | 1.265                            | -0.011 | 2.14   | 1.265                            | 0.098  | 2.14   |
| 11            | 14            | UDSTL5              | 1.134                            | 0.047  | -1.577 | 1.134                            | -0.094 | -1.577 |
| 12            | 14            | UDSTL5              | -1.934                           | 0.003  | -0.038 | -1.934                           | 0.003  | -0.038 |
| 17            | 14            | UDSTL5              | 1.131                            | -0.05  | 1.521  | 1.131                            | 0.091  | 1.521  |
| 11            | 14            | UDSTL6              | 1.83                             | -0.029 | -2.35  | 1.83                             | -0.091 | -2.35  |
| 12            | 14            | UDSTL6              | -3.042                           | 0.002  | 0.044  | -3.042                           | -0.001 | 0.044  |
| 17            | 14            | UDSTL6              | 1.832                            | 0.027  | 2.407  | 1.832                            | 0.092  | 2.407  |
| 11            | 14            | UDSTL7              | 1.674                            | 0.009  | -2.526 | 1.674                            | -0.07  | -2.526 |
| 12            | 14            | UDSTL7              | -2.728                           | 0.003  | -0.67  | -2.728                           | -0.004 | -0.67  |
| 17            | 14            | UDSTL7              | 1.759                            | -0.011 | 1.559  | 1.759                            | 0.075  | 1.559  |
| 11            | 14            | UDSTL8              | 1.121                            | 0.008  | -1.175 | 1.121                            | -0.1   | -1.175 |
| 12            | 14            | UDSTL8              | -1.964                           | 0.001  | 0.677  | -1.964                           | 0.006  | 0.677  |
| 17            | 14            | UDSTL8              | 1.036                            | -0.009 | 2.145  | 1.036                            | 0.094  | 2.145  |
| 11            | 14            | UDSTL9              | 0.818                            | 0.071  | -1.206 | 0.818                            | -0.088 | -1.206 |
| 12            | 14            | UDSTL9              | -1.423                           | 0.003  | -0.065 | -1.423                           | 0.004  | -0.065 |
| 17            | 14            | UDSTL9              | 0.814                            | -0.074 | 1.114  | 0.814                            | 0.084  | 1.114  |



### 5.5 *Transforming forces into applicable joint loads*

In order to be able to apply the forces extracted from the building model to the joint model, resisted forces (F1, F2, F3, M1, M2 and M3) need to be transformed into applicable point forces (F1A, F2A, F3A; F1B, F2B and F3B). Moments (M1, M2 and M3) are transformed by simple geometric processes into applied forces, with a characteristic direction and sign. Once the magnitudes equivalent to the moments are obtained, they are added vectorially where they correspond to the magnitudes of forces (F1, F2 and F3) in the original model (Table 4 and Table 5).

### 5.6 *Calculation and analysis of model type A*

Once the mechanical properties, forces and support conditions of the model have been applied, it is analysed using Sap2000 V.20 software. A static linear calculation is performed for each of the load cases applied. The parameters analysed are: maximum absolute Von Mises stresses and deformations.

### 5.7 *Support conditions and application of loads*

To analyse Von Mises stresses, fixed support conditions are used at the end of bar 12, while the loads corresponding to bars 11 and 17 are applied to their respective flanges. To analyse deformations, fixed support conditions are used at the ends of bars 12 and 17, while their respective forces are applied to bar 11 (Table 6).

### 5.8 *Von Mises analysis*

When analysing the maximum absolute Von Mises stresses, the aim is to find areas where forces are concentrated which may jeopardise the stability of the parts, and to make the respective geometric amendments to counteract the tendencies observed. Knowing that the nominal yield strength ( $f_y$ ) of S355 steel is equal to 355 N/mm<sup>2</sup>, the stress analysis is done graphically with a range between 100 N/mm<sup>2</sup> and 355 N/mm<sup>2</sup> (Table 7).

### 5.9 *Deformation analysis*

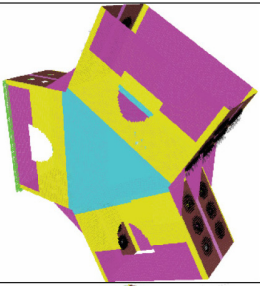
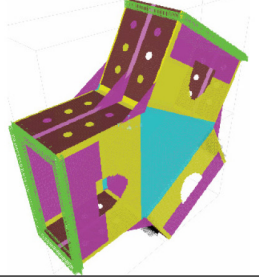
The deformation analysis seeks to ensure that the displacement of the joint arms does not affect the correct functioning of the general structure to which they belong (Table 8 and Figure 12).

## 6. **Description of the joint type A model**

The model consists of three parts made of S355 steel, a central part (TYPE A) that acts as a skeleton and two twin parts (TYPE B) that cover the first part symmetrically on each side.

The result of the design process resolves the articulations of the bars forming the joint in such a way that the joint has radial symmetry and bilateral symmetry.



|                                |  |   |
|--------------------------------|--|---|
| Model type A / 12.<br>(VMS)    |  | Forces applied to<br>11A and 11B.<br>17A and 17B. |
| Model type A / 12-17.<br>(Def) |  | Forces applied to<br>11A and 11B.                 |

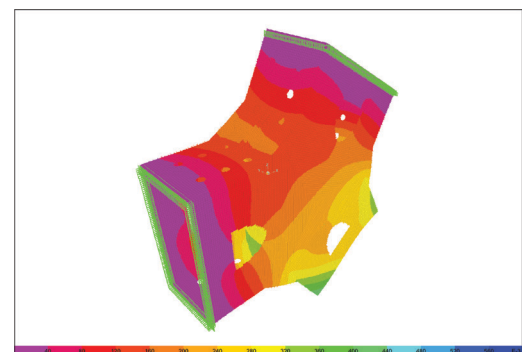
**Table 6.**

Joint type model with supports and applied forces for Von Mises stress and deformation analysis

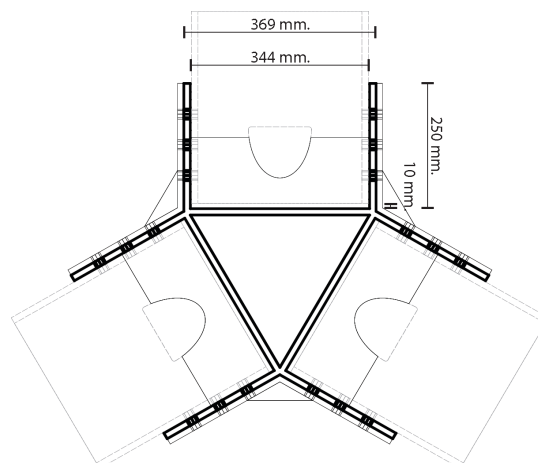
| Maximum deformation in mm. |                     |           |           |                   |
|----------------------------|---------------------|-----------|-----------|-------------------|
| Model:                     | 12 17 (Free bar 11) |           |           |                   |
| Case                       | Max def X           | Max def Y | Max def Z | Max resulting def |
| UDSTL10                    | 0.449               | -0.165    | -0.341    | 0.588             |
| UDSTL2                     | 0.323               | -0.132    | -0.267    | 0.439             |
| UDSTL3                     | 0.331               | -0.117    | -0.315    | 0.471             |
| UDSTL4                     | 0.316               | -0.148    | -0.220    | 0.412             |
| UDSTL5                     | 0.238               | -0.117    | -0.214    | 0.341             |
| UDSTL6                     | 0.410               | -0.149    | -0.321    | 0.541             |
| UDSTL7                     | 0.318               | -0.111    | -0.331    | 0.472             |
| UDSTL8                     | 0.292               | -0.151    | -0.174    | 0.372             |
| UDSTL9                     | 0.166               | -0.098    | -0.164    | 0.253             |

**Table 8.**

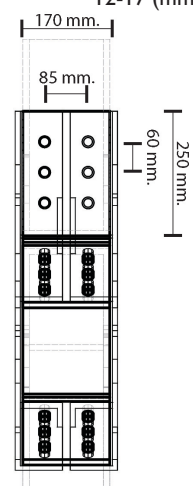
Maximum deformation joint type / 12-17

**Figure 12.**

Maximum resulting deformation UDSTL10 model type / 12-17 (mm)

**Figure 13.**

Type A part, plan view

**Figure 14.**

Type A part, elevation view

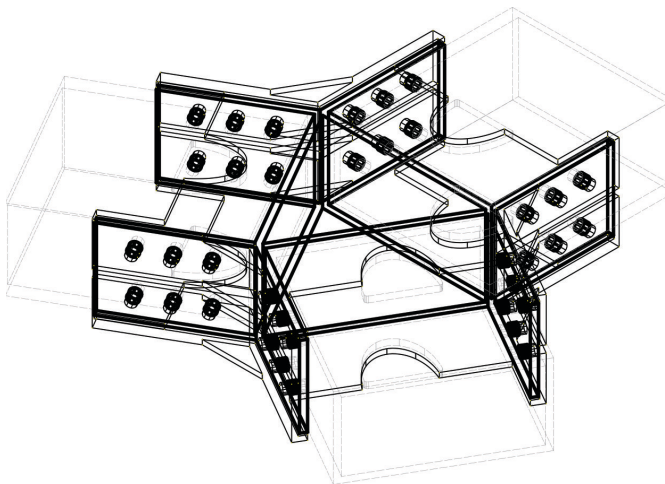


**Figure 15.**  
Type A part, axonometric

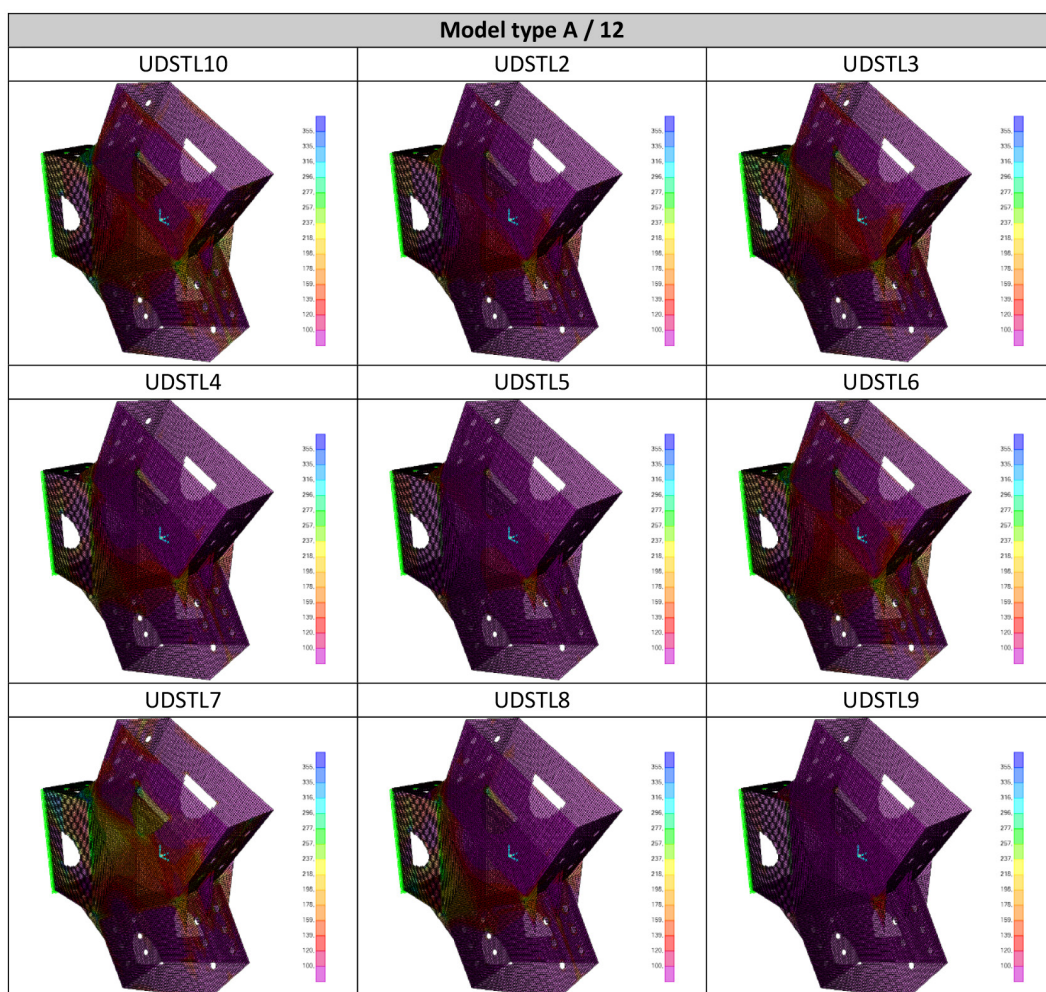


**Table 7.**  
Maximum absolute SVM stress analysis (n/mm<sup>2</sup>)



### 6.1 *Type A part*

The core of the part is three steel plates welded together to form an equilateral triangle. This triangle has three symmetrical arms, each made up of two steel plates with three pairs of holes that help, through bolts and pins, to connect the bars to the parts of the joint (Figure 13, Figure 14 and Figure 15).

### 6.2 *Type B part*

The part comprises a large steel plate, the shape of which resembles a triangle that covers and goes beyond the surface of the type A part and appendages, of the same material and thickness, symmetrically located on each of the arms of the joint (Figure 16, Figure 17 and Figure 18).

These appendages or flanges are perforated in such a way that their holes coincide in number, position and length with the holes of the type A part and extend longitudinally beyond the limits of the superficial steel plate. The type A part is attached to two type B parts and to the bars by means of screws screwed under pressure. In addition, each arm of the joint includes a pin in the pair of holes furthest from the centre, which acts as a pivot to allow the necessary rotation of the bars (Figure 19 and Figure 20).

## 7. Application of the folding system

The foldability of the system is achieved by creating an articulation in each of the three arms thanks to a pin allowing each of the bars to be rotated. Releasing the free type B part makes it possible for the bars to rotate 90°, going from a vertical position (folded) to a horizontal position (deployed). The type B part is then repositioned and secured (Figure 21, Figure 22, Figure 23 and Figure 24).

## 8. Conclusion

- The proposed joint allows for packing of the framing bars, which means that the structure will be easier to prefabricate and transport.
- When we move away from the field of lightweight structures, the geometry of the joint mechanism is subordinate to its structural functioning, so that the joint must be capable of supporting and efficiently transferring the building's own forces.
- The right balance between the resistance of parts and the simplicity of the mechanism has led us to look for a design that avoids superfluous use of materials.
- In response, we have tried to reduce to a minimum the number of joint parts and ensure that they have dual purpose, hence the choice of the position of the pins to achieve articulation, or the shape of the type B part, which serves to stop the joint moving during transport.
- Despite not having a connection with the slabs, joint number 14 of the building model is chosen as we are seeking a joint that is representative due to concentration of forces, but at the same time avoids elevating the complexity of the model by introducing shear forces to the joint.
- In the Von Mises stress analysis it is observed that, for almost all load cases, the material stress is below 30% of the allowable stress, and that the concentration of stress is centred on the angle formed by the joint arms.
- With the support conditions applied, the maximum deformations at the ends of the arms should be taken as a trend rather than an absolute value.

- The deformations follow a pattern similar to that shown by the bar model of the building to which this joint belongs.
- More complex finite element models need to be created and non-linear calculations applied to understand the plastic behaviour of the parts in greater depth.
- The efficiency of the design lies in how compact the joint can be. This is easier to achieve if the stresses from the bars have magnitudes that allow them to be distributed among the least number of bolts possible, which means that the system works best for low buildings with less load.

#### Notes

- (1) See London City Hall (2002), Swiss Re (2001-2003) and Hearst Tower (2003-2006).
- (2) "Hexagonal architecture does not form a single flow in history, nor has it ever generated a dominant trend. However, looking back upon it now, we might perhaps say that these designs have always played the role of posing an antithesis to the main current".
- (3) "Honeycomb Tube Architecture: The spatial potentialities of hexagons" (2007).
- (4) "Honeycomb Dynamics Architecture" (2008).
- (5) "Honeycomb Tube Architecture Technology" (2009).
- (6) Locking Means for tripods (TORR., 1917).
- (7) Hub Assembly for Collapsible Structure (Beaulieu, 1986).
- (8) Tent System Employing an Improved Spider Hub and Associated Frame Structure and Method of Compacting the Frame for Reduced Storage Size (Samuel, 2018).
- (9) Self-locking joint for folding structures (Pérez Valcárcel, et al., 2018).
- (10) Autodesk AutoCAD 2017.
- (11) In this case, SAP2000 V.19 software has been chosen.

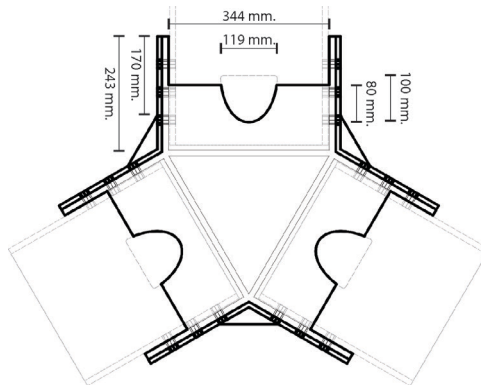


**Figure 16.**  
Type B part, plan view

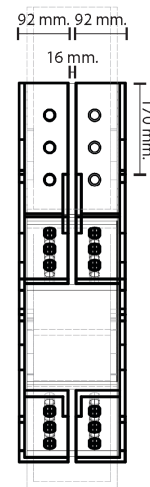


**Figure 17.**  
Type B part, elevation view

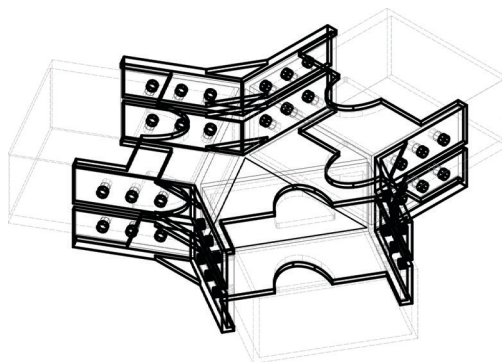


**Figure 18.**  
Type B part, axonometric

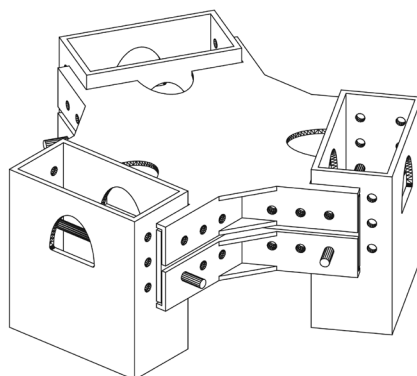


**Figure 19.**  
Joint with bars folded, axonometric

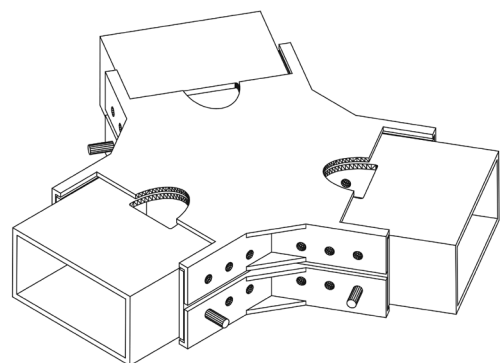


**Figure 20.**  
Joint with bars deployed, axonometric



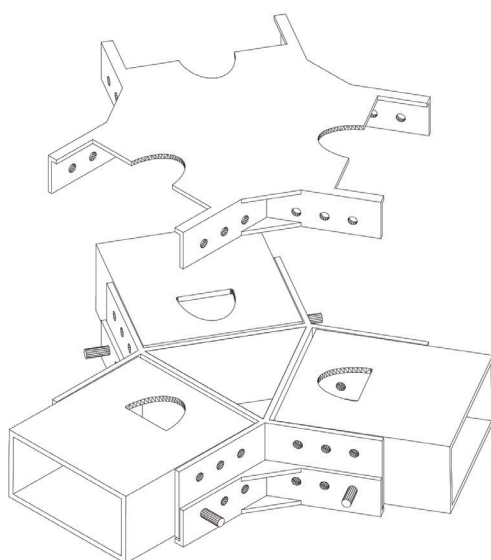


**Figure 21.**  
Folding process 1, axonometric

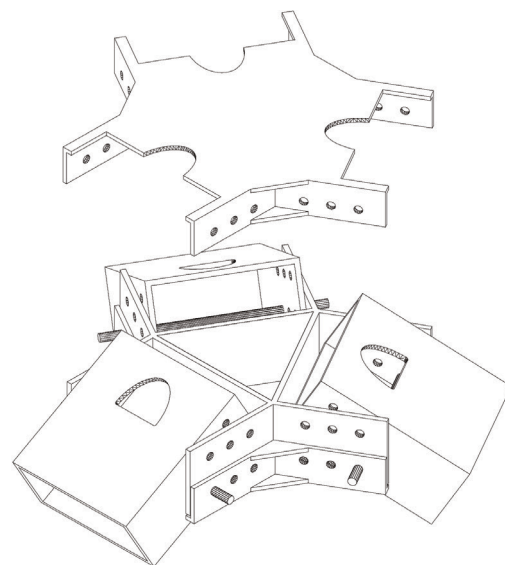


**Figure 22.**  
Folding process 2, axonometric

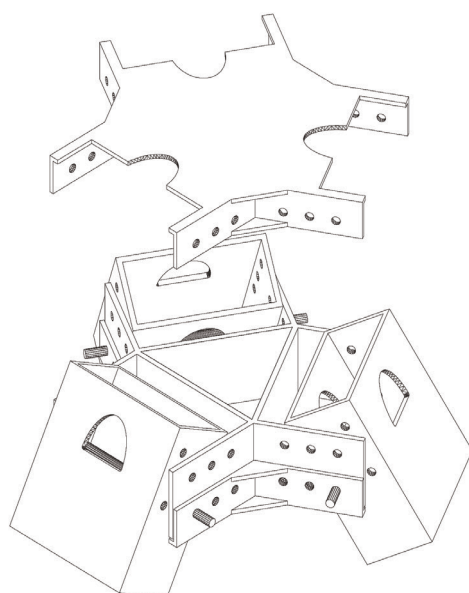


**Figure 23.**  
Folding process 3, axonometric

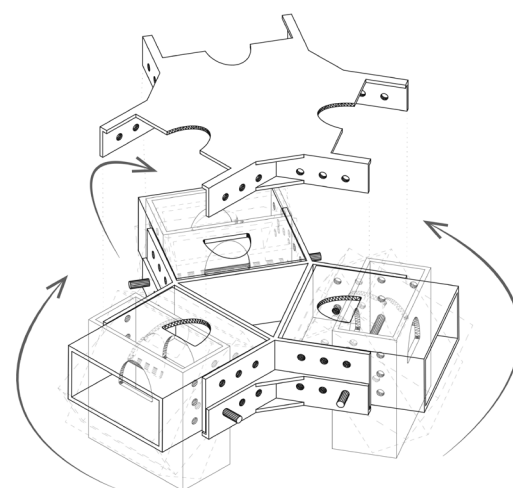


**Figure 24.**  
Bar deployment process, axonometric

## References

- Beaulieu, B. J., 1986. United States, Patent No. US4627210.
- Boake, T., 2013. *Diagrid Structures: Innovation and Detailing*. Portugal, s.n.
- Candela, F. et al., 1993. *Arquitectura Transformable*. Sevilla: Escuela Técnica Superior de Arquitectura de Sevilla.
- Cantos, H., 2015. *Mallas Desplegables Sometidas a Compresión*. Barcelona: Universidad Politécnica de Cataluña.
- Chen, Y., 2003. *Design of Structural Mechanisms*. Oxford: University of Oxford.
- de Meijer, J., 2012. *Lateral Stiffness of Hexagrid Structures*. Eindhoven: Eindhoven University of Technology.
- Escrig, F., 2013. *Modular, ligero, transformable. Un paseo por la arquitectura ligera móvil*. Sevilla: Universidad de Sevilla.
- Franco, R., 2010. *Hacia una Arquitectura móvil*. Bogotá: Universidad Jorge Tadeo Lozano.
- Goldsmith, M., 1953. *The Tall Building: The Effects of Scale*. Chicago: Illinois Institute of Technology.
- Hales, T. C., 1999. The Honeycomb Conjecture. [Online] Available at: <https://arxiv.org/abs/math/9906042>.
- Hales, T. C., 1999. The Honeycomb Conjecture. *Discrete and Computational Geometry*, p. 25.
- HTA Association, 2007. *Honeycomb Tube Architecture*. In: Tokyo: s.n., p. 32.
- HTA Association, 2007. *Honeycomb Tube Architecture*. Tokyo: HTA Association.
- HTA Association, 2008. *Honeycomb Dynamics Architecture*. Tokyo: HTA Association.
- HTA Association, 2009. *Honeycomb Tube Architecture Technology*. Tokyo: HTA Association.
- Korsavi, S. & Maqhareh, M. R., 2014. The Evolutionary Process of Diagrid Structure Towards Architectural, Structural and Sustainability Concepts: Reviewing Case Studies. *Architectural Engineering Technology*, Volume 3.
- Montuori, G. M., 2015. *Innovative Structural Solutions for Tall Buildings*. Naples: University of Naples Federico II.
- Montuori, G. M., Fadda, M., Perrella, G. & Mele, E., 2015. Hexagrid - Hexagonal tube structures for tall buildings: patterns, modeling and design. *The Structural Design of Tall and Special Buildings*.
- Pérez Valcárcel, J., Muñoz Vidal, M., López César, I. & Suárez Riestra, F., 2018. España, Patent No. ES2653648 B2.
- Samuel, F. L., 2018. United States, Patent No. US9976319 B2.



Torr., J. G., 1917. United States, Patent No. US1226724.

Weisstein, E. W., 2001. Honeycomb Conjecture. [Online] Available at: <http://mathworld.wolfram.com/HoneycombConjecture.html>